

## THE CHANGING FACE OF THE EXTRASOLAR GIANT PLANET HD 209458b

JAMES Y-K. CHO,<sup>1,2</sup> KRISTEN MENO,<sup>3,4,5</sup> BRADLEY M. S. HANSEN,<sup>3,6,7</sup> AND SARA SEAGER<sup>2,8</sup>

Received 2002 September 11; accepted 2003 February 28; published 2003 March 20

### ABSTRACT

High-resolution atmospheric flow simulations of the tidally locked extrasolar giant planet HD 209458b show large-scale spatio-temporal variability. This is in contrast to the simple, permanent day/night (i.e., hot/cold) picture. The planet’s global circulation is characterized by a polar vortex in motion around each pole and a banded structure corresponding to approximately three broad zonal (east-west) jets. For very strong jets, the circulation-induced temperature difference between moving hot and cold regions can reach up to  $\sim 1000$  K, suggesting that atmospheric variability could be observed in the planet’s spectral and photometric signatures.

*Subject headings:* planetary systems — planets and satellites: general — stars: atmospheres — turbulence

### 1. INTRODUCTION

Roughly 100 gaseous giant planets are currently known to orbit nearby Sun-like stars.<sup>9</sup> Many of those planets are located at very small orbital distances from their parent stars, where tidal forces are thought to maintain a rotation rate synchronous with the orbit—thus producing permanent day and night sides on the planet. This situation presents a new regime of atmospheric circulation, not encountered in our solar system: slowly rotating giant planets, which are continuously exposed to intense stellar heating on the same side. Measuring the resulting temperature structure on these planets is a major goal of current and future observational programs. In this Letter, we report on high-resolution, fully turbulent global simulations of the atmospheric flow on HD 209458b, presently the only close-in extrasolar giant planet (CEGP) with a measured mass ( $M_p$ ) and radius ( $R_p$ ).

The parent star of HD 209458b shows discernible brightness decrements every 3.5 days, due to occultations by the planet as it transits across the star. This property has recently led to precise measurements of  $M_p$  and  $R_p$  (Charbonneau et al. 2000; Henry et al. 2000; Mazeh et al. 2000), confirming its giant nature. It has also allowed the detection of sodium absorption, providing the first probe of the planet’s atmosphere (Charbonneau et al. 2002). According to the standard planetary formation picture, HD 209458b is expected to have formed at a large distance ( $>1$  AU) from its parent star (see, e.g., Boss 1996) and migrated inward (Goldreich & Tremaine 1980; Lin, Bodenheimer, & Richardson 1996; Murray et al. 1998), quickly ( $\leq 10$  Myr) reaching its present distance of only 0.046 AU from the star (see, e.g., Burrows et al. 2000). There, it was forced by tidal effects to permanently present the same face to

its star (see, e.g., Goldreich & Soter 1966)—as the Moon does to the Earth. From this synchronization, the rotation period of the CEGP is known (same as its orbital period of 3.5 days). However, unlike our Moon with its insignificant atmosphere, HD 209458b is expected to possess vigorous meteorology and associated horizontal transport of heat and chemical species, owing to the presence of a thin, stable (radiative) atmospheric region above the convective interior (Guillot et al. 1996; Seager & Sasselov 1998).

### 2. MODEL

We model the stable region of HD 209458b’s atmosphere as a shallow layer of hydrostatically balanced, frictionless gas—moving under the influence of gravitational and Coriolis accelerations. The motion of such a layer enveloping a planet is governed by the equivalent barotropic formulation of the shallow-water equations on a rotating sphere (Salby 1989):

$$\frac{\partial \mathbf{v}}{\partial t} + \mathbf{v} \cdot \nabla \mathbf{v} = -g \nabla h - f \mathbf{k} \times \mathbf{v} + \mathcal{F}_a, \quad (1)$$

$$\frac{\partial h}{\partial t} + \mathbf{v} \cdot \nabla h = -\mathcal{K} h \nabla \cdot \mathbf{v} + \mathcal{F}_d, \quad (2)$$

where  $\mathbf{v} = \mathbf{v}(\lambda, \varphi, t)$  is the horizontal velocity, with  $\lambda$  and  $\varphi$  the longitude and latitude, respectively;  $h = h(\lambda, \varphi, t)$  is the thickness of the modeled layer, proportional to the temperature;  $f = 2\Omega \sin \varphi$  is the Coriolis parameter, where  $\Omega$  is the rotation rate of the planet;  $\mathbf{k}$  is the local unit vector normal to the planetary surface;  $g$  is the gravitational acceleration;  $\mathcal{F}_a = -g \nabla \eta [1 - \exp(-t/\tau_a)] \cos \varphi \cos \lambda$  and  $\mathcal{F}_d = -(h - h_E)/\tau_d$  are, respectively, the adiabatic and diabatic thermal forcing, representing uneven hemispheric heating and cooling due to synchronization;  $\tau_a$  and  $\tau_d$  are characteristic  $e$ -folding times;  $h_E = H + \eta \cos \varphi \cos \lambda$  is the equilibrium thickness;  $\eta$  and  $H$  are constants; and  $\mathcal{K} = R/c_p$ , where  $R$  is the specific gas constant and  $c_p$  is the specific heat at constant pressure.

The nonlinear equations (1) and (2) describe circulations in which the motion field is vertically aligned over one or more pressure scale heights,  $H_p$ . They are a column-integrated representation of the equations used in general circulation models and are solved numerically using the highly accurate pseudo-spectral algorithm (Eliassen, Mechenhauer, & Rasmussen 1970; Orszag 1970). Approximately 150 simulation runs with up to T341 ( $1024 \times 512$  grid) resolution have been performed to explore the full physical and numerical parameter-space available

<sup>1</sup> Spectral Sciences, Inc., 99 South Bedford Street, No. 7, Burlington, MA 01803.

<sup>2</sup> Current address: Department of Terrestrial Magnetism, Carnegie Institution of Washington, 5241 Broad Branch Road, NW, Washington, DC 20015.

<sup>3</sup> Department of Astrophysical Sciences, Princeton University, Peyton Hall, Princeton, NJ 08540.

<sup>4</sup> Chandra Fellow.

<sup>5</sup> Current address: Department of Astronomy, University of Virginia, P.O. Box 3818, Charlottesville, VA 22903.

<sup>6</sup> Division of Astronomy, University of California at Los Angeles, 8971 Math Sciences, Los Angeles, CA 90095.

<sup>7</sup> Hubble Fellow.

<sup>8</sup> School of Natural Sciences, Institute for Advanced Study, 1 Einstein Drive, Princeton, NJ 08540.

<sup>9</sup> See, e.g., <http://www.obspm.fr/encycl/encycl.html> and <http://exoplanets.org/almanacframe.html>.

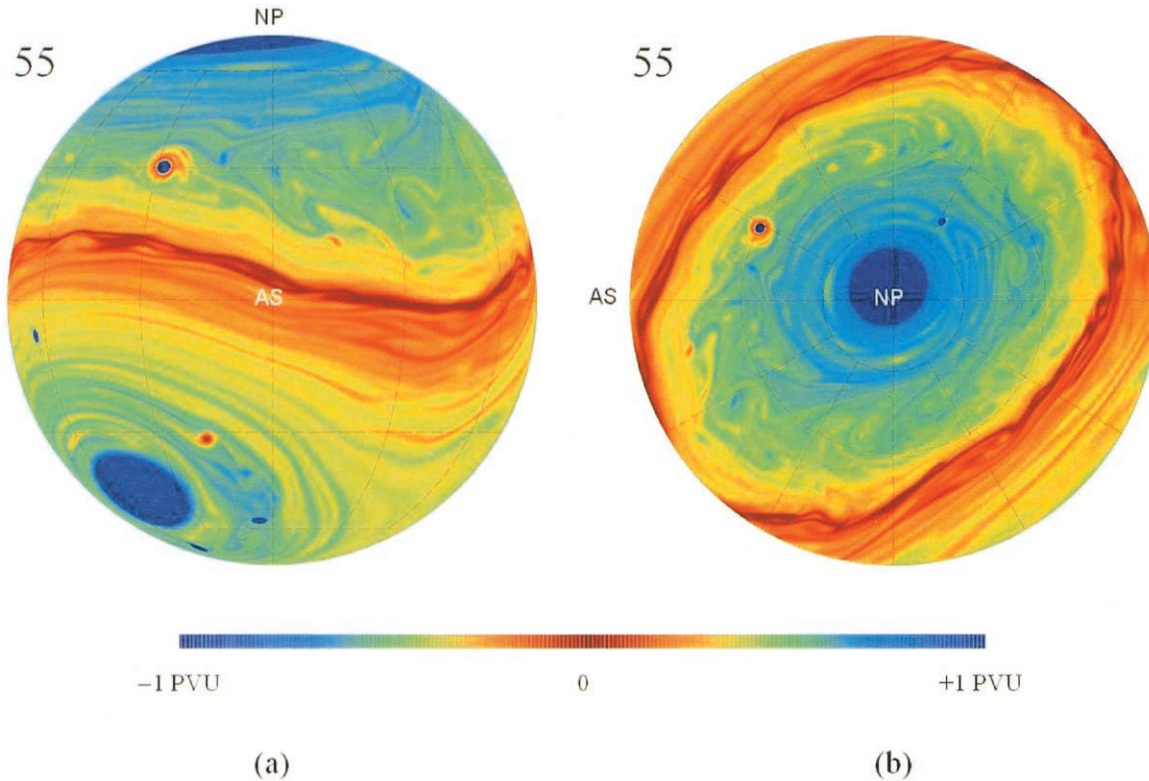


FIG. 1.—Two views of the dynamical flow tracer, potential vorticity (Holton 1992), at day (=year) 55 from our T341 ( $1024 \times 512$  grid resolution) simulation of the atmospheric circulation of HD 209458b: (a) orthographic projection centered at the antistellar (AS) point on the night side and (b) polar-stereographic projection centered at the north pole (NP). 1 PVU =  $4 \times 10^{-27} \text{ s}^{-1} \text{ m}^{1/\kappa}$ . The global flow is characterized by two circumpolar cyclonic (rotating in the same direction as the planet—counterclockwise in the figure) vortices at high latitudes and high-amplitude planetary waves at low latitudes.

for the HD 209458b atmosphere. The details of the full exploration will be described elsewhere (J. Y-K. Cho, K. Menou, B. M. S. Hansen, & S. Seager 2003, in preparation). Here we emphasize only the main robust features from the large number of simulations—namely, the emergence of long-timescale variability due to moving polar vortices and “thermal” spots of high contrast from the background temperature field.

High-resolution, shallow-layer barotropic models in spherical geometry have been successfully used to model the atmospheric dynamics of the solar system gaseous giant planets (Williams 1978; Cho & Polvani 1996a) as well as stratospheric (stable region) phenomena on the Earth (see, e.g., Juckes & McIntyre 1987). An alternate model of observed cloud level circulation on Jupiter as a surface expression of deep convective columns, oriented parallel to the planetary rotation axis, also exists (Sun, Schubert, & Glatzmeier 1993; Schubert & Zhang 2000). However, only the shallow-layer model has thus far qualitatively reproduced the essential features (bands, zonal winds, persistent spots, and anticyclonic dominance) on all of the giant planets in our solar system using only the observed values of physical parameters (Cho & Polvani 1996a).

For HD 209458b, we adopt parameter values where known (Charbonneau et al. 2000; Henry et al. 2000; Mazeh et al. 2000):  $\mathcal{K} = 0.29$ ,  $g = 8 \text{ m s}^{-2}$ ,  $R_p = 10^8 \text{ m}$ ,  $\Omega = 2.1 \times 10^{-5} \text{ s}^{-1}$ , and  $H = 2 \times 10^6 \text{ m}$ . The last ( $=H_p/\mathcal{K}$ ) represents the global mean layer thickness, whose value corresponds to the equivalent blackbody temperature ( $T_{\text{atm}} \approx 1400 \text{ K}$  for a Bond albedo,  $A = 0.2$ ; the results presented here, however, are insensitive to the precise choice of  $T_{\text{atm}}$  and  $A$ ). The values for two required parameters— $\eta$ , the amplitude of hemispheric thermal forcing, and  $U$ , the characteristic wind speed related to the

global mean kinetic energy—are not known and hence varied. From run to run,  $\eta$  is varied from 0 to  $0.4H$ , corresponding, respectively, to no heating and maximum substellar-point heating in the absence of atmospheric motion;  $U$  is varied from 50 to  $1000 \text{ m s}^{-1}$ , roughly the observed value for Jupiter (Ingersoll 1990) and the value expected from a simple thermal wind balance (Showman & Guillot 2002), respectively. Note that the latter value leads to a nonlinearly balanced wind field that can locally approach the sound speed ( $\sim 2700 \text{ m s}^{-1}$ ); on all observed atmospheres in our solar system,  $U$  does not exceed  $\sim 400 \text{ m s}^{-1}$  (Beatty & Chaiken 1990). We have carefully studied the effects of  $U$  on the variability and thermal contrast and find that, while a variability in the flow is a generic feature for HD 209458b, a significant thermal contrast generally requires a small  $\eta$  or a large  $U$ . In the following, we give an example of the expected generic flow pattern and then describe a typical flow-induced thermal variability that may be observationally relevant.

### 3. RESULTS

Figure 1 shows an instantaneous atmospheric flow field on HD 209458b at dynamic equilibrium from one of our simulations with  $U = 400 \text{ m s}^{-1}$  and  $\eta$  corresponding to a maximum day/night temperature difference of 180 K. The flow exhibits considerable complexity and variability: it is characterized by a broad equatorial band containing thin, undulating filamentary structures at low and middle latitudes and displaced, translating circumpolar vortices at the rotation poles. The large undulations at low latitudes, which can roll up into small vortices, are due to high-amplitude Rossby (planetary) waves. In addition to

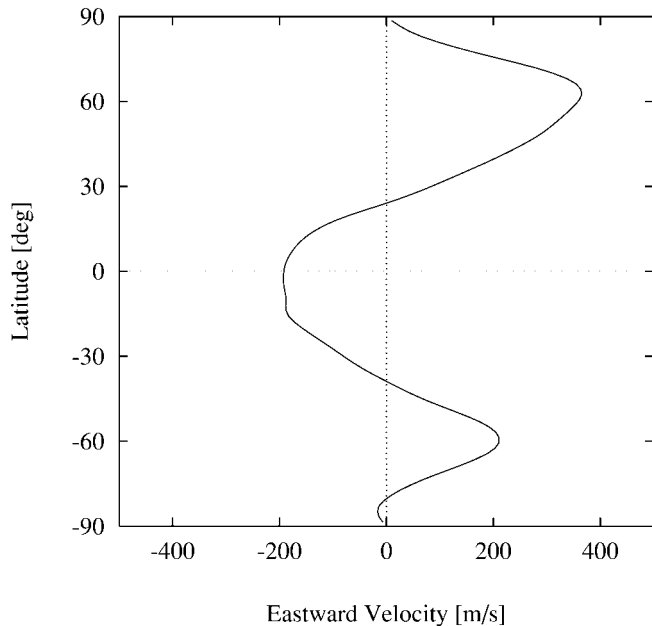


FIG. 2.—Steady circulation profile from the flow of Fig. 1: longitudinally averaged zonal (eastward) wind velocity. Zonal jets emerge from a random initial condition owing to conversion of small-scale stirring/eddies to planetary waves in the atmosphere (as seen in Fig. 1), a generic feature of shallow-layer turbulence under differential (latitudinally dependent) rotation  $f$ . This basic profile has emerged approximately at day 20 of the simulation and does not change for the duration of the simulation (several hundred HD 209458b days). On HD 209458b, the jets are fewer, broader, and stronger than those observed on Jupiter. This is because HD 209458b is hotter and rotating more slowly than Jupiter. Hemispheric thermal forcing is applied on this robust flow.

being responsible for weather, the planetary waves efficiently stir and mix tracers (e.g., clouds, chemical species, potential vorticity) when they break, homogenizing the region in which the breakings occur (Jukes & McIntyre 1987). In contrast, polar vortices sequester air inside, their sharp boundaries serving as robust barriers to material transport between their interiors and the well-mixed interstitial regions. The overall flow is similar to that of Earth’s winter stratosphere.

The complex flow of Figure 1 corresponds to a global circulation pattern of three zonal jets, shown in Figure 2. Jets are atmospheric flow structures, which are obtained by longitudinally averaging the eastward wind at each latitude. The pattern in Figure 2 naturally evolves from an initially random flow without jets, with the basic profile forming approximately at day 20. The emergence of jets from a random field is a generic feature of turbulent flows in a differentially rotating shallow layer (Rhines 1975; Williams 1978; Cho & Polvani 1996b). For the extreme values of  $U$  considered with all other parameters held fixed, two or four jets are also possible. However, once formed, the jets do not change qualitatively—even under applied thermal forcing—for up to several hundred HD 209458b days, the duration of the simulation.

The presence of a low number of broad jets, along with polar vortices, leads to a circulation pattern that is markedly different from that of cloud-top Jupiter. Although CEGPs are sometimes dubbed “hot Jupiters,” the circulation pattern is more like that of Uranus or Neptune, or even Earth, than that of Jupiter or Saturn, which have  $\sim 10$  narrow jets (Ingersoll 1990). Dynamically, this is expected given roughly the factors of 10 greater  $T_{\text{atm}}$  and 10 slower rotation rate of HD 209458b compared to Jupiter. The combined effect, giving the flows in Figures 1 and

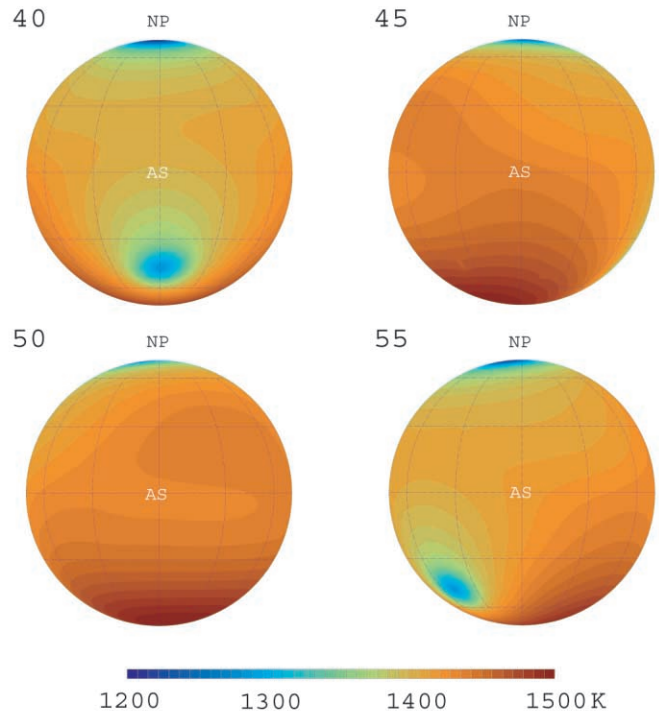


FIG. 3.—Four successive nighttime views of the temperature field in orthographic projection (on HD 209458b days indicated). A persistent “thermal dipole,” associated with the circumpolar vortices, revolves around the pole and provides high thermal contrasts that may be detectable in the planet’s observational signatures. In contrast to the simple, permanent day/night picture, the hottest atmospheric region is, at times, on the night side of the planet. These spots are long-lived, asymmetric (cold regions are more well defined and have larger amplitude), and can serve as large areas of atmosphere with distinct chemistry and thermodynamics. The global equilibrium blackbody temperature of the atmosphere is taken to be 1400 K.

2, is characterized by the Rossby deformation scale,  $L_D = (KgH)^{1/2}/f$ , which is to be compared with  $R_p$ . Generally,  $L_D/R_p \ll 1$  is required for a Jupiter-like multiple-jet circulation pattern without pronounced polar vortices at the cloud-top. For HD 209458b,  $L_D/R_p \sim 1$ .

Jets and vortices/eddies can strongly influence the overall thermal structure by transporting heat. Since the state of the HD 209458b cloud-top is not likely to be at rest and driven solely by stellar heating, we delay the application of thermal forcing (in contrast to Showman & Guillot 2002) until the flow field self-organizes into the pattern in Figure 2. Dynamically, this is a likely flow state of HD 209458b in the presence of weak or uniform heating (i.e., at *presynchronization*). The forcing is slowly increased to the specified value of  $\eta$  over a characteristic radiative equilibrium time,  $\tau_r = 10$  days, appropriate for  $\sim 1$  bar pressure level on HD 209458b. At this depth,  $\tau_r \gg \tau_c$  (where  $\tau_c = R_p/U$  is the characteristic circulation time), signifying a large distance advection of air mass before it warms or cools appreciably. The results presented here do not change qualitatively with the value of  $\tau_r$  ( $\sim 0$ –100 days), using either an adiabatic ( $\mathcal{F}_a$ ,  $\tau_a = \tau_r$ ) or a diabatic ( $\mathcal{F}_d$ ,  $\tau_d = \tau_r$ ) representation of thermal forcing.

At each point on the planet, the layer thickness is related to the temperature field,  $T(\lambda, \varphi, t) = hg/c_p$ , via the hypsometric relation (Holton 1992; Salby 1989). In our simulations with small  $\eta$  or large  $U$ , the  $T$  field exhibits a generic feature that is in direct contrast to the simple permanent day/night picture. Figure 3 shows the  $T$  distribution (from the same run of Figs. 1 and 2)

at several different times. Note that the warmest and the coldest regions are not located at the substellar and the antistellar “thermal poles” (at the equator), respectively. Instead, the temperature extrema are located near the rotation poles, inside a coherent hot/cold spot pair at each pole. Nor are the extrema stationary: they revolve around the poles with a period of  $\sim 25$  days in this case. The movement leads to a distribution that for a time has the temperature minimum actually on the “hot” day side and the maximum on the “cold” night side. In addition, the temperature difference between the two extrema is large and strongly asymmetric; here the difference is  $\sim 300$  K, with the diffuse hot region  $\sim 70$  K above and the sharp cold region  $\sim 230$  K below  $T_{\text{atm}}$ . For the case with  $U = 1000 \text{ m s}^{-1}$ , the difference reaches  $\sim 1000$  K, with a temperature minimum of  $\sim 800$  K below  $T_{\text{atm}}$  at the core of the cold spots.

#### 4. DISCUSSION

The presence of high-contrast hot and cold spots on HD 209458b induces spatio-temporal variability, which may produce detectable fluctuations in observational signatures. Sensitive enough infrared flux measurements (e.g., those possible with *SIRTF*) could reveal variability in time during an orbit of the planet as different faces are seen from Earth, as well as from orbit to orbit as the spots (polar vortices) revolve about the rotation poles. The lack of detectable variability would thus point toward either an obscuring uniform haze overlying the modeled region or an inefficient conversion of stellar irradiation to atmospheric kinetic energy. In the latter case, the formed spots are weak (i.e., small temperature/thickness perturbation) and thermal forcing that produces bulging in the modeled layer of more than several percent overwhelms any temperature variability due to atmospheric motion. The equilibrium day/night temperature is then robustly maintained.

The extreme conditions inside the spots in our calculations suggest several additional potential observables since absorption levels, albedo, intrinsic thermal emission, and presence, type, or height of clouds could all be different within the different spots. The spatially integrated spectrum, therefore, can be different from the uniform planet case. For example, enhanced levels of  $\text{CH}_4/\text{CO}$  abundance inside the cold spots are possible, given the value of  $T_{\text{atm}}$  used (Seager, Whitney, & Sasselov 2000). Similarly, condensates, such as  $\text{MgSiO}_3$  (enstatite), may also be found inside the diffuse hot spots, where temperatures may be high enough (Sudarsky, Burrows, & Pinto 2000; Seager et al. 2000). If the temperature at radiative equilibrium is actually higher than assumed (e.g.,  $\sim 2000$  K), the opposite situation may occur— $\text{MgSiO}_3$  may be found in the cold spots. In addition, by sequestering chemically active species and periodically exposing them to the stellar irradiation (as the spots revolve around the poles), the spots could also affect atomic number densities and could be part of the explanation for the recently observed low abundance of Na I on HD 209458b (Charbonneau et al. 2002).

J. Y.-K. C. acknowledges the hospitality of the Institute for Advanced Study, where the initial part of this work was completed, and R. Levine for helpful discussions. K. M. is supported by NASA under Chandra Fellowship grant PF9-10006, awarded by the Smithsonian Astrophysical Observatory for NASA under contract NAS8-39073. B. M. S. H. is supported by Hubble Fellowship grant HF-01120.01-99A, awarded by the Space Telescope Science Institute, which is operated by the Association of Universities for Research in Astronomy, Inc., for NASA under contract NAS5-26555. S. S. is supported by the W. M. Keck foundation. We thank the referee, W. Hubbard, for comments.

#### REFERENCES

- Beatty, J. K., & Chaiken, J. 1990, *The New Solar System* (3d ed.; Cambridge: Cambridge Univ. Press)
- Boss, A. P. 1996, *ApJ*, 469, 906
- Burrows, A., et al. 2000, *ApJ*, 534, L97
- Charbonneau, D., Brown, T. M., Latham, D. W., & Mayor, M. 2000, *ApJ*, 529, L45
- Charbonneau, D., Brown, T. M., Noyes, R. W., & Gilliland, R. L. 2002, *ApJ*, 568, 377
- Cho, J. Y.-K., & Polvani, L. M. 1996a, *Science*, 273, 335
- . 1996b, *Phys. Fluids*, 8, 1531
- Eliassen, E., Mechenhauer, B., & Rasmussen, E. 1970, *Copenhagen Univ., Inst. Teoretisk Meteorologi, Tech. Rep. 2*
- Goldreich, P., & Soter, S. 1966, *Icarus*, 5, 375
- Goldreich, P., & Tremaine, S. 1980, *ApJ*, 241, 425
- Guillot, T., Burrows, A., Hubbard, W. B., Lunine, J. I., & Saumon, D. 1996, *ApJ*, 459, L35
- Henry, G., Marcy, G. W., Butler, R. P., & Vogt, S. S. 2000, *ApJ*, 529, L41
- Holton, J. R. 1992, *An Introduction to Dynamic Meteorology* (San Diego: Academic)
- Ingersoll, A. P. 1990, *Science*, 248, 308
- Jukes, M. N., & McIntyre, M. E. 1987, *Nature*, 328, 590
- Lin, D. N. C., Bodenheimer, P., & Richardson, D. C. 1996, *Nature*, 380, 606
- Mazeh, T., et al. 2000, *ApJ*, 532, L55
- Murray, N., Hansen, B., Holman, M., & Tremaine, S. 1998, *Science*, 279, 69
- Orszag, A. 1970, *J. Atmos. Sci.*, 27, 890
- Rhines, P. B. 1975, *J. Fluid Mech.*, 69, 417
- Salby, M. L. 1989, *Tellus*, 41A, 48
- Schubert, G., & Zhang, K. 2000, in *ASP Conf. Ser. 212, From Giant Planets to Cool Stars*, ed. C. A. Griffith & M. S. Marley (San Francisco: ASP), 210
- Seager, S., & Sasselov, D. D. 1998, *ApJ*, 502, L157
- Seager, S., Whitney, B. A., & Sasselov, D. D. 2000, *ApJ*, 540, 504
- Showman, A. P., & Guillot, T. 2002, *A&A*, 385, 166
- Sudarsky, D., Burrows, A., & Pinto, A. A. 2000, *ApJ*, 538, 885
- Sun, Z.-P., Schubert, G., & Glatzmeier, G. A. 1993, *Science*, 260, 661
- Williams, G. P. 1978, *J. Atmos. Sci.*, 35, 1399